Vietnam Journal of Mechanics, Vol. 46, No. 4 (2024), pp. 343 – 353
DOI: https://doi.org/10.15625/0866-7136/21137

HIGHER-ORDER STOCHASTIC AVERAGING FOR INVESTIGATING A VEHICLE SUSPENSION SYSTEM WITH NONLINEAR DAMPING AND STIFFNESS

Nguyen Dong Anh[1,2], **Nguyen Ngoc Linh**[3], **Nguyen Duc Ngoc**[3], **Nguyen Van Manh**[4]
[1]*Institute of Mechanics, Vietnam Academy of Science and Technology, Hanoi, Vietnam*
[2]*University of Engineering and Technology, Vietnam National University, Hanoi, Vietnam*
[3]*Faculty of Mechanical Engineering, Thuyloi University, Hanoi, Vietnam*
[4]*Faculty of Mechanical, Hanoi University of Civil Engineering, Hanoi, Vietnam*
[*]E-mail: manhnv@huce.edu.vn

Received: 14 March 2024 / Revised: 22 April 2024 / Accepted: 29 June 2024
Published online: 22 October 2024

Abstract. The paper deals with a quarter-car model with nonlinear damping and stiffness under white noise base excitation using the higher-order stochastic averaging method for analyzing approximate responses. Recently, a novel higher-order averaging procedure has been developed to find analytically the first-, second-, and third-order stationary joint probability density functions (PDF) of amplitude and full phase by solving the corresponding Fokker–Planck–Kolmogorov (FPK) equation, and it will be extended to the nonlinear quarter-car model. Accordingly, the mean-square responses such as the displacement, and velocity of the sprung mass can be obtained analytically. The influences of excitation intensity on the dynamic responses, as well as the variations of linear and nonlinear damping, are analyzed. A very satisfactory agreement is found between the accuracy of the solutions corresponding to higher-order stochastic averaging and that of Monte Carlo simulation.

Keywords: higher-order stochastic averaging (HOSA), quarter car model, nonlinear suspension, random excitation.

1. INTRODUCTION

In the literature, a linear vehicle suspension system is just an approximation of a real vehicle and is not an accurate representation. Major sources of nonlinearity in a such system are geometric effects resulting in not linear effective springs, asymmetric and/or complex damping, tire separation, and bump stops [1, 2]. Namely, for real vehicles, the

suspension springs are usually installed in inclined directions at some offset from the centers of the tires. Additionally, they are often supported by a set of suspension arms or linkages that rotate around a pivot and do not move in a precisely linear direction. This means the motion ratio of the spring and the wheel center does not remain constant along with wheel travel. In other words, since the effective spring stiffness is not constant, then a linear spring model is inaccurate. Automotive dampers are inherently nonlinear due to the damping mechanism derived from fluid orifices in a passive system, as well as from variable orifice valves for tuning the damping effect in a semi-active and/or active system [2,3]. Tire separation and bump stops also make the system nonlinear due to the impact effects, and they often lead to transient responses when compared to long-term responses involving nonlinear restoring and damping effects.

Among simplified quarter-car models of the vehicle suspension system, the two-degree-of-freedom (2-DOF) quarter-car model and the single-degree-of-freedom (SDOF) quarter-car model are often used [4–9]. The first one is used for studying the effects of nonlinear damping and/or restoring on the responses of the sprung and unsprung masses [4–6]. Meanwhile, the second one involves a case where the tire stiffness is very large compared to that of the suspension spring. In other words, the SDOF quarter-car model is a reduced model of the 2DOF one when omitting the unsprung mass. Hence, the SDOF quarter-car model is used to investigate nonlinear damping and/or restoring effects on the sprung mass [4,7–9]. Focusing the attention on the nonlinear SDOF quarter-car model, it is seen that there are two typical base excitations, harmonic and stochastic ones. In [4], the effect of a cubic damping characteristic on the system is investigated under the steady-state sinusoidal base input. The analytical solutions are obtained using the harmonic balance method and validated with direct numerical integration. In [7], the suspension system with cubic nonlinear damping and spring under multi-frequency periodic excitation from the road surface is investigated for possible chaotic motion. In the case of stochastic base excitation, [8] investigates an SDOF quarter-car model with the signum function of damping subjected to white or colored noise excitation. The Fokker–Planck–Kolmogorov (FPK) equation is expanded in terms of generalized Hermite polynomials and subsequently solved by a Galerkin method. In [9], the considered damping effect is asymmetrical, and the system is excited by the road roughness of ISO standard. The mean displacement of the sprung mass is numerically investigated.

Recently, a higher-order stochastic averaging (HOSA) procedure using the FPK equation was developed by Anh et al. [10, 11] and then applied to the Van der Pol oscillator [12], mono-stable Duffing piezoelectric energy harvesting system under white noise excitation [13]. The key factor of HOSA is the transient response, stability, and reliability of the systems, and the intrinsic nonlinearity in the original system is retained in the

averaged system [13]. Until now, no extension of HOSA has been performed to analyze dynamical systems including both nonlinear damping and stiffness.

In the paper, HOSA is further applied to the SDOF quarter-car model with nonlinear damping and stiffness under white noise excitation. The outline of this paper is organized as follows. The implementation of the procedure for this model is presented in Section 2. The analytical expression of the first-, second-, and third-order probability density functions (PDFs) are also given in this section. In Section 3, numerical examination is carried out, and the accuracy of the approximate responses is verified by the result of the Monte Carlo method. The conclusion is presented in Section 4.

2. APPLICATION OF HIGH ORDER AVERAGING METHOD TO VEHICLE SUSPENSION WITH NONLINEAR STIFFNESS AND DAMPING

Consider an SDOF quarter-car model with a nonlinear spring and a nonlinear damper [7] as shown in Fig. 1.

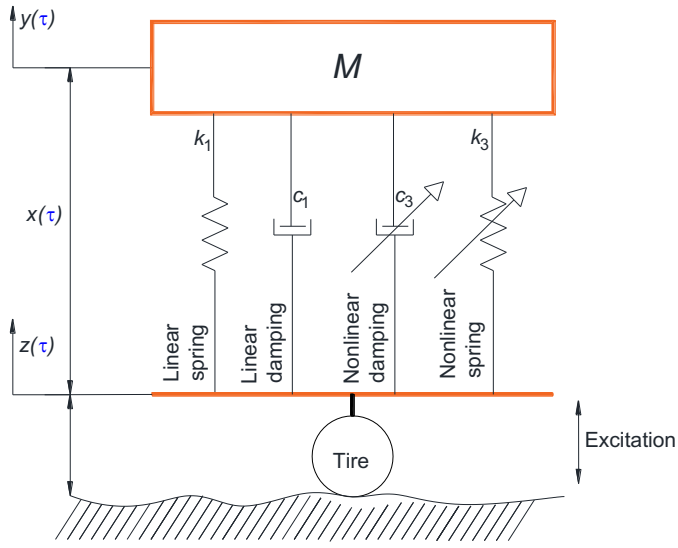

Fig. 1. Single DOF quarter-car suspension model

The motion equation of the system in terms of the suspension travel variable is

$$M\frac{\mathrm{d}^2x}{\mathrm{d}\tau^2}+c_1\frac{\mathrm{d}x}{\mathrm{d}\tau}+c_3\left(\frac{\mathrm{d}x}{\mathrm{d}\tau}\right)^3+k_1x+k_3x^3=-M\ddot{z}, \tag{1}$$

where the over dots denote the derivatives with respect to time τ, M is the sprung mass, k_1 and k_3 are the linear elastic coefficient and nonlinear cubic stiffness coefficient of the

spring, c_1 and c_3 are linear damping coefficient and nonlinear damping coefficient, respectively, $\ddot{z}$ is the base excitation, y is the vertical displacement of the sprung mass and $x = y - z$ is the relative displacement (suspension travel) between the sprung mass and wheel. Let's set

$$t = \omega_n \tau, \quad \omega_n^2 = \frac{k_1}{M}, \quad \varepsilon\lambda_1 = \frac{c_1}{2M\omega_n}, \quad \varepsilon\lambda_3 = \frac{c_3}{2M}\omega_n, \quad \varepsilon\beta_3 = \frac{k_3}{M\omega_n^2}, \quad \omega_0^2 = 1. \tag{2}$$

Eq. (1) is transformed to the following form

$$\ddot{x} + \omega_0^2 x = \varepsilon f(x, \dot{x}) + \sqrt{\varepsilon}\sigma\xi(t), \tag{3}$$

where the over dots now denote derivatives with respect to dimensionless time t,

$$f(x, \dot{x}) = -\left(2\lambda_1\dot{x} + 2\lambda_3\dot{x}^3 + \beta_3 x^3\right), \tag{4}$$

and $-\ddot{z}/\omega_n^2 = \sqrt{\varepsilon}\sigma\xi(t)$, σ is the white noise intensity, the small parameter ε, $0 < \varepsilon < 1$, represents the weak excitation, the $\xi(t)$ represents the excitation acceleration being a zero mean Gaussian white noise process with unit intensity

$$E\left(\xi(\bar{t})\,\xi(\bar{t} + \bar{\tau})\right) = \delta(\bar{\tau}). \tag{5}$$

The operator E denotes the mathematical expectation, $\delta(\bar{\tau})$ is the Dirac–Delta function. Without loss of generality, the small parameter ε is also added to the restoring and damping elements, and the solution of the corresponding linear system (3) (equivalent to $\varepsilon = 0$) has the form

$$x(t) = a\cos\phi, \quad \dot{x}(t) = -a\omega_0\sin\phi, \quad \phi = \omega_0 t + \varphi, \tag{6}$$

where a is the amplitude and φ is the phase angle. In the linear case, they are constants. Otherwise, they are functions of time $a(t), \phi(t)$ in the nonlinear case. Following HOSA [11, 13], the system of Ito stochastic differential equations for amplitude and full phase can be obtained from Eq. (3)

$$\begin{aligned} \mathrm{d}a(t) &= \varepsilon K_1(a,\phi)\mathrm{d}t - \sqrt{\varepsilon}\frac{\sigma}{\omega}\sin\phi\,\mathrm{d}B(t), \\ \mathrm{d}\phi(t) &= (\omega + \varepsilon K_2(a,\phi))\mathrm{d}t - \sqrt{\varepsilon}\frac{\sigma}{a\omega}\cos\phi\,\mathrm{d}B(t), \end{aligned} \tag{7}$$

where $B(t)$ is a Wiener process, $\xi(t) = \mathrm{d}B(t)/\mathrm{d}t$, and

$$\begin{aligned} K_1(a,\phi) &= \left[\begin{array}{l} \dfrac{\sigma^2}{4a\omega_0^2} - \lambda_1 a - \dfrac{3}{4}a^3\lambda_3\omega_0^2 + \left(\lambda_1 a + \dfrac{\sigma^2}{4a\omega_0^2} + a^3\lambda_3\omega_0^2\right)\cos 2\phi \\ + \dfrac{\beta_3}{4\omega_0}a^3\sin 2\phi + \dfrac{\beta_3}{8\omega_0}a^3\sin 4\phi - \dfrac{1}{4}a^3\lambda_3\omega_0^2\cos 4\phi \end{array}\right], \\ K_2(a,\phi) &= \left[\begin{array}{l} \dfrac{3\beta_3}{8\omega_0}a^2 - \left(\lambda_1 + \dfrac{\sigma^2}{2a^2\omega_0^2} + \dfrac{1}{2}a^2\lambda_3\omega_0^2\right)\sin 2\phi + \dfrac{\beta_3}{2\omega_0}a^2\cos 2\phi \\ + \dfrac{\beta_3}{8\omega_0}a^2\cos 4\phi + \dfrac{1}{4}a^2\lambda_3\omega_0^2\sin(4\phi) \end{array}\right]. \end{aligned} \tag{8}$$

Accordingly, the FPK equation, written for the PDF of amplitude and phase $W(a,\phi)$, has the form

$$\begin{aligned}\omega_0\frac{\partial W}{\partial \phi} &= -\varepsilon\frac{\partial}{\partial a}(K_1(a,\phi)W) - \varepsilon\frac{\partial}{\partial \phi}(K_2(a,\phi)W)\\ &+ \frac{\varepsilon}{2}\left[\frac{\partial^2}{\partial a^2}(K_{11}(a,\phi)W) + 2\frac{\partial^2}{\partial a\partial\phi}(K_{12}(a,\phi)W) + \frac{\partial^2}{\partial \phi^2}(K_{22}(a,\phi)W)\right],\end{aligned} \tag{9}$$

where $K_1(a,\phi), K_2(a,\phi)$ are given by Eq. (8) and

$$\begin{aligned}&K_{11}(a,\phi) = \sigma^2\sin^2\phi/\omega_0^2, \quad K_{12}(a,\phi) = \sigma^2\sin\phi\cos\phi/(a^2\omega_0^2),\\ &K_{22}(a,\phi) = \sigma^2\sin^2\phi/\omega_0^2,\end{aligned} \tag{10}$$

Then the approximate PDF of Eq. (9) is determined in the form of a series with respect to the small parameter as follows

$$W(a,\phi) = W_0(a)\left\{1 + \varepsilon\left[W_{10}(a) + W_{11}(a,\phi)\right] + \varepsilon^2\left[W_{20}(a) + W_{22}(a,\phi)\right] + \ldots\right\}, \tag{11}$$

where $W_0(a), W_{10}(a), W_{20}(a)$ are functions of only a; $W_{11}(a,\phi), W_{22}(a,\phi)$ are arbitrary functions of (a,ϕ). Substituting (11) into (9) and comparing the coefficients of $\varepsilon^0, \varepsilon^1, \varepsilon^2, \ldots$ in both sides of the obtained result, yields

$$\varepsilon^0 : \omega_0\frac{\partial W_0(a,\phi)}{\partial \phi} = 0, \tag{12}$$

$$\varepsilon^1 : \omega_0\frac{\partial W_1}{\partial \phi} = -\frac{\partial}{\partial a}(K_1W_0) - \frac{\partial}{\partial \phi}(K_2W_0) + \frac{1}{2}\left[\frac{\partial^2}{\partial^2 a}(K_{11}W_0) + 2\frac{\partial^2}{\partial a\partial\phi}(K_{12}W_0) + \frac{\partial^2}{\partial^2\phi}(K_{22}W_0)\right], \tag{13}$$

$$\varepsilon^2 : \omega_0\frac{\partial W_2}{\partial \phi} = -\frac{\partial}{\partial a}(K_1W_1) - \frac{\partial}{\partial \phi}(K_2W_1) + \frac{1}{2}\left[\frac{\partial^2}{\partial^2 a}(K_{11}W_1) + 2\frac{\partial^2}{\partial a\partial\phi}(K_{12}W_1) + \frac{\partial^2}{\partial^2\phi}(K_{22}W_1)\right]. \tag{14}$$

It is noted that $W_0(a)$ is determined from the first-order averaging procedure corresponding to Eq. (12) for the order of ε^0. One has

$$\frac{\partial}{\partial a}\left[\left(\frac{\sigma^2}{4a\omega_0^2} - \lambda_1 a - \frac{3}{4}a^3\lambda_2\omega_0^2\right)W_0(a)\right] - \frac{1}{2}\frac{\partial^2}{\partial a^2}\left[\frac{\sigma^2}{2\omega^2}W_0(a)\right] = 0, \tag{15}$$

which gives the first-order PDF for amplitude

$$W_0(a) = Ca\exp\left\{-\left(\lambda_1 + \frac{3}{4}a^2\lambda_3\omega_0^2\right)\frac{2\omega_0^2}{\sigma^2}a^2\right\}. \tag{16}$$

This shows that $W_0(a)$ contains all coefficients of linear terms, say λ_1 and ω_0, as well as that of the cubic damping terms λ_3, but excludes the coefficient β_3 of the cubic stiffness. Thus, the effect of the cubic stiffness is lost during the implementation of the

first-order stochastic averaging procedure. That is the major disadvantage of this procedure.

Next, substituting (8), (10) and (16) into (13) and integrating this equation with respect to the variable ϕ leads to

$$W_1(a,\phi) = W_0(a)\left[W_{10}(a) + W_{11}(a,\phi)\right], \tag{17}$$

where

$$\begin{aligned} W_{10}(a) &= (27a^{10}\beta_3\lambda_3^2\omega_0^6)/(160\sigma^4) - (a^6\beta_3\lambda_3\omega_0^2)/(2\sigma^2) \\ &\quad - (3a^4\beta_3\lambda_1)/(8\sigma^2) + (9a^8\beta_3\lambda_1\lambda_3\omega_0^4)/(64\sigma^4), \end{aligned} \tag{18}$$

$$\begin{aligned} W_{11}(a,\phi) = &-\frac{a^4\beta_3\left(3a^2\lambda_3\omega_0^2 + 2\lambda_1\right)\left(4\cos(2\phi) + \cos(4\phi)\right)}{16\sigma^2} \\ &+ \frac{a^4\lambda_3\omega_0^3\left(3a^2\lambda_3\omega_0^2 + 2\lambda_1\right)\left(4\sin(2\phi) + \sin(4\phi)\right)}{8\sigma^2}. \end{aligned} \tag{19}$$

Next, substituting (8), (10) and (16) into (14) and integrating this equation with respect to the variable leads to the second-order PDF

$$W_2(a,\phi) = W_0(a)\left[W_{20}(a) + W_{22}(a,\phi)\right], \tag{20}$$

where

$$W_{20}(a) = \begin{bmatrix} (a^{16}(-2871\beta_3^2\lambda_3^3\omega_0^8 + 9180\lambda_3^5\omega_0^{14}))/(40960\sigma^6) \\ -(a^{10}(-10980\lambda_1\beta_3^2\lambda_3\omega_0^2\sigma^2 + 97680\lambda_1\lambda_3^3\omega_0^8\sigma^2))/(25600\sigma^6) \\ -(a^4(-11520\lambda_1^2\lambda_3\omega_0^2\sigma^4 + 31680\lambda_3^2\omega_0^2\sigma^6))/(10240\sigma^6) \\ +(a^{12}(-1240\beta_3^2\lambda_1^2\lambda_3\omega_0^4 + 10575\beta_3^2\lambda_3^2\omega_0^4\sigma^2 + 4080\lambda_1^2\lambda_3^3\omega_0^{10} - 94140\lambda_3^4\omega_0^{10}\sigma^2))/(30720\sigma^6) \\ -(a^8(-2800\beta_3^2\lambda_1^2\sigma^2 + 2250\beta_3^2\lambda_3\sigma^4 + 24640\lambda_1^2\lambda_3^2\omega_0^6\sigma^2 - 152280\lambda_3^3\omega_0^6\sigma^4))/(20480\sigma^6) \\ +(a^{14}(-3828\lambda_1\beta_3^2\lambda_3^2\omega_0^6 + 12240\lambda_1\lambda_3^4\omega_0^{12}))/(35840\sigma^6) - (3a^2\lambda_1\lambda_3)/4 + (6a^6\lambda_1\lambda_3^2\omega_0^4)/\sigma^2 \end{bmatrix}, \tag{21}$$

$$W_{22}(a,\phi) = \begin{bmatrix} P_1(a)\sin(2\phi) + P_2(a)\sin(4\phi) + P_3(a)\sin(6\phi) \\ +P_4(a)\cos(2\phi) + P_5(a)\cos(4\phi) + P_6(a)\cos(6\phi) + P_7(a)\cos(8\phi) \end{bmatrix}, \tag{22}$$

$$P_1(a) = \begin{bmatrix} -(324\beta_3a^{16}\lambda_3^4\omega_0^{12} + 486\beta_3a^{14}\lambda_1\lambda_3^3\omega_0^{10} + 180\beta_3a^{12}\lambda_1^2\lambda_3^2\omega_0^8 - 2040\beta_3a^{12}\lambda_3^3\omega_0^8\sigma^2 \\ -2440\beta_3a^{10}\lambda_1\lambda_3^2\omega_0^6\sigma^2 - 720\beta_3a^8\lambda_1^2\lambda_3\omega_0^4\sigma^2 + 1500\beta_3a^8\lambda_3^2\omega_0^4\sigma^4 + 720\beta_3a^6\lambda_1\lambda_3\omega_0^2\sigma^4 \\ +720\beta_3a^4\lambda_3\sigma^6)/(1280\omega_0^1\sigma^6) \end{bmatrix}, \tag{23}$$

$$P_2(a) = \begin{bmatrix} -(162\beta_3a^{16}\lambda_3^4\omega_0^{12} + 243\beta_3a^{14}\lambda_1\lambda_3^3\omega_0^{10} + 90\beta_3a^{12}\lambda_1^2\lambda_3^2\omega_0^8 - 210\beta_3a^{12}\lambda_3^3\omega_0^8\sigma^2 \\ -140\beta_3a^{10}\lambda_1\lambda_3^2\omega_0^6\sigma^2 + 300\beta_3a^8\lambda_3^2\omega_0^4\sigma^4 + 240\beta_3a^6\lambda_1\lambda_3\omega_0^2\sigma^4 + 120\beta_3a^4\lambda_3\sigma^6)/(2560\omega_0^1\sigma^6) \end{bmatrix}, \tag{24}$$

$$P_3(a) = -(180\beta_3a^8\lambda_3^2\omega_0^4\sigma^4 + 120\beta_3\lambda_1a^6\lambda_3\omega_0^2\sigma^4)/(3840\omega_0^1\sigma^6), \tag{25}$$

$$P_4(a) = \left[\begin{array}{l} -(162a^{16}\beta_3^2\lambda_3^3\omega_0^9 + 243a^{14}\beta_3^2\lambda_1\lambda_3^2\omega_0^7 + 90a^{12}\beta_3^2\lambda_1^2\lambda_3\omega_0^5 - 840a^{12}\beta_3^2\lambda_3^2\omega_0^5\sigma^2 \\ +4680a^{12}\lambda_3^4\omega_0^{11}\sigma^2 - 980a^{10}\beta_3^2\lambda_1\lambda_3\omega_0^3\sigma^2 + 6240a^{10}\lambda_1\lambda_3^3\omega_0^9\sigma^2 - 280a^8\beta_3^2\lambda_1^2\omega_0\sigma^2 \\ +150a^8\beta_3^2\lambda_3\omega_0\sigma^4 + 2080a^8\lambda_1^2\lambda_3^2\omega_0^7\sigma^2 - 14160a^8\lambda_3^3\omega_0^7\sigma^4 - 11280a^6\lambda_1\lambda_3^2\omega_0^5\sigma^4 - \\ -1920a^4\lambda_1^2\lambda_3\omega_0^3\sigma^4 + 5280a^4\lambda_3^2\omega_0^3\sigma^6 + 960a^2\lambda_1\lambda_3\omega_0\sigma^6)/(1280\omega_0^1\sigma^6) \end{array} \right], \tag{26}$$

$$P_5(a) = \left[\begin{array}{l} (735a^{12}\beta_3^2\lambda_3^2\omega_0^5\sigma^2 - (243a^{14}\beta_3^2\lambda_1\lambda_3^2\omega_0^7)/2 - 45a^{12}\beta_3^2\lambda_1^2\lambda_3\omega_0^5 - 81a^{16}\beta_3^2\lambda_3^3\omega_0^9 \\ +360a^{12}\lambda_3^4\omega_0^{11}\sigma^2 + 910a^{10}\beta_3^2\lambda_1\lambda_3\omega_0^3\sigma^2 + 480a^{10}\lambda_1\lambda_3^3\omega_0^9\sigma^2 + 280a^8\beta_3^2\lambda_1^2\omega_0\sigma^2 \\ -180a^8\beta_3^2\lambda_3\omega_0\sigma^4 + 160a^8\lambda_1^2\lambda_3^2\omega_0^7\sigma^2 + \\ +600a^8\lambda_3^3\omega_0^7\sigma^4 + 480a^6\lambda_1\lambda_3^2\omega_0^5\sigma^4 - 240a^4\lambda_3^2\omega_0^3\sigma^6)/(2560\omega_0^1\sigma^6) \end{array} \right], \tag{27}$$

$$P_6(a) = \left[\begin{array}{l} (270a^{12}\beta_3^2\lambda_3^2\omega_0^5\sigma^2 + 1080a^{12}\lambda_3^4\omega_0^{11}\sigma^2 + 360a^{10}\beta_3^2\lambda_1\lambda_3\omega_0^3\sigma^2 + 1440a^{10}\lambda_1\lambda_3^3\omega_0^9\sigma^2 \\ +120a^8\beta_3^2\lambda_1^2\omega_0\sigma^2 - 90a^8\beta_3^2\lambda_3\omega_0\sigma^4 + 480a^8\lambda_1^2\lambda_3^2\omega_0^7\sigma^2 - 720a^8\lambda_3^3\omega_0^7\sigma^4 \\ -240a^6\lambda_1\lambda_3^2\omega_0^5\sigma^4)/(3840\omega_0^1\sigma^6) \end{array} \right], \tag{28}$$

$$P_7(a) = \left[\begin{array}{l} (45a^{12}\beta_3^2\lambda_3^2\omega_0^5\sigma^2 + 180a^{12}\lambda_3^4\omega_0^{11}\sigma^2 + 60a^{10}\beta_3^2\lambda_1\lambda_3\omega_0^3\sigma^2 + 240a^{10}\lambda_1\lambda_3^3\omega_0^9\sigma^2 \\ +20a^8\beta_3^2\lambda_1^2\omega_0\sigma^2 - 15a^8\beta_3^2\lambda_3\omega_0\sigma^4 + 80a^8\lambda_1^2\lambda_3^2\omega_0^7\sigma^2 - 60a^8\lambda_3^3\omega_0^7\sigma^4)/(5120\omega_0^1\sigma^6) \end{array} \right]. \tag{29}$$

Finally, substituting (16), (17), and (20) into (11) one obtains the third-order PDF

$$W(a,\phi) = Ca\exp\left(-\frac{2\omega_0^2}{\sigma^2}a^2\lambda_1 - \frac{3\omega_0^4}{2\sigma^2}a^4\lambda_3\right)\left[1 + \varepsilon W_{10}(a) + \varepsilon W_{11}(a,\phi) + \varepsilon^2 W_{20}(a) + \varepsilon^2 W_{22}(a,\phi)\right], \tag{30}$$

where $W_{10}(a), W_{11}(a,\phi), W_{20}(a), W_{22}(a,\phi), C$ are given in (18), (19), (21), (22) and C is the normalization coefficient determined from the condition

$$\int_0^\infty \mathrm{d}a \int_0^{2\pi} W(a,\phi)\mathrm{d}\phi = 1. \tag{31}$$

Using the obtained third-order PDF (30), the second moment of the displacement and velocity of the sprung mass in Eq. (3) can be calculated by, respectively

$$\langle x^2\rangle = \frac{1}{C}\int_0^\infty \mathrm{d}a \int_0^{2\pi} a^2\cos^2\phi W(a,\phi)\mathrm{d}\phi, \tag{32}$$

$$\langle \dot{x}^2\rangle = \frac{1}{C}\int_0^\infty \mathrm{d}a \int_0^{2\pi} a^2\omega_0^2\sin^2\phi W(a,\phi)\mathrm{d}\phi. \tag{33}$$

In the next section, the first-, second-, and third-order stationary joint PDFs will be investigated and the accuracy of the corresponding responses will be verified by Monte Carlo simulations.

3. NUMERICAL RESULTS AND DISCUSSION

In this section, the numerical examination of the suspension system (3) is carried out where the first-, second-, and third-order PDFs given by (17), (20), (30) will be analyzed, as well as the corresponding mean-square displacements of the sprung mass. Besides, the accuracy of those approximate displacements will be compared to the ones obtained by the Monte Carlo method. The input parameters are taken as presented in Table 1, the small parameter is $\varepsilon = 0.1$, the vehicle velocity is $v = 14$ (m/s), and the road roughness is adapted from ISO 8608:2016 [14] which leads to various values of the excitation intensity σ.

Table 1. Input parameter values

Nomenclature	Parameter	Value
Sprung mass (kg)	M	240
Linear stiffness coefficient (N/m)	k_1	1.5×10^4
Nonlinear stiffness coefficient (N/m^3)	k_3	1.6×10^4
Linear damping coefficient (Ns/m)	c_1	7000
Nonlinear damping coefficient (Ns^3/m^3)	c_3	50

Time histories of the displacements of the sprung mass corresponding to the road classes A and H (see Table 2) are exhibited in Figs. 2 and 3 using the Monte Carlo method. The maximum displacement amplitude is about 0.015 as $\sigma = 53.8 \times 10^{-4}$ (Fig. 2), and 0.82 as $\sigma = 3445.2 \times 10^{-4}$ (Fig. 3). The mean-square values of the displacement related to those road classes, say $\langle x^2 \rangle_{MC}$, are presented in Table 2.

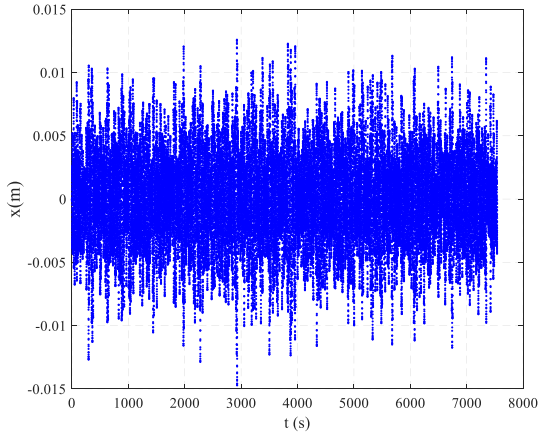

Fig. 2. Time histories of the displacement response with $\sigma = 53.8 \times 10^{-4}$

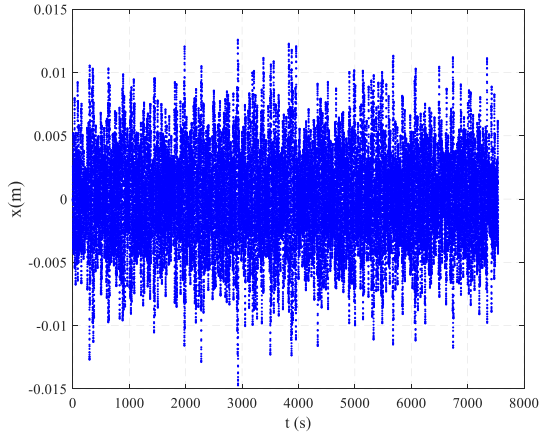

Fig. 3. Time histories of the displacement response with $\sigma = 3445.2 \times 10^{-4}$

Table 2. The errors of the mean-square displacement with various values of σ

Road class	σ $\times 10^{-4}$	$\langle x^2 \rangle_{MC}$ $\times 10^{-4}$	$\langle x^2 \rangle_1$ $\times 10^{-4}$	Error (%)	$\langle x^2 \rangle_2$ $\times 10^{-4}$	Error (%)	$\langle x^2 \rangle_3$ $\times 10^{-4}$	Error (%)
A (Very good)	53.80	0.121	0.1210	0.4176	0.1210	0.4176	0.1210	0.4179
B (Good)	107.59	0.482	0.4820	0.1507	0.4820	0.1493	0.4820	0.1493
C (Average)	215.19	1.930	1.930	0.1425	1.930	0.1367	1.930	0.1367
D (Poor)	430.60	7.710	7.720	0.1412	7.720	0.1180	7.720	0.1181
F	861.30	30.830	30.89	0.1823	30.86	0.0895	30.86	0.0900
G	1722.6	122.86	123.26	0.3269	122.81	0.0427	122.81	0.0376
H	3445.2	483.82	488.62	0.9926	481.56	0.4673	481.88	0.4015

Figs. 4 and 5 present the contours of the third-order PDF curve $W(a,\phi)$ given by Eq. (30) in the aW-plane with ten values of the linear damping coefficient λ_1 and ten values of the nonlinear damping coefficient λ_3, respectively. The considered road roughness is of class F, and $\omega_0 = 1, \beta_3 = 0.1$. In general, as λ_1 decreases and λ_3 is unchanged (see Fig. 4), the $W(a,\phi)$ curve gets wider and the peaks move forward strongly along the a-axis. On the other hand, as λ_3 varies and λ_1 is unchanged (see Fig. 5), the influence of the cubic damping on the shape of the $W(a,\phi)$ curve is not much. It is seen that the third-order PDF curve has the same shape as the Rayleigh distribution.

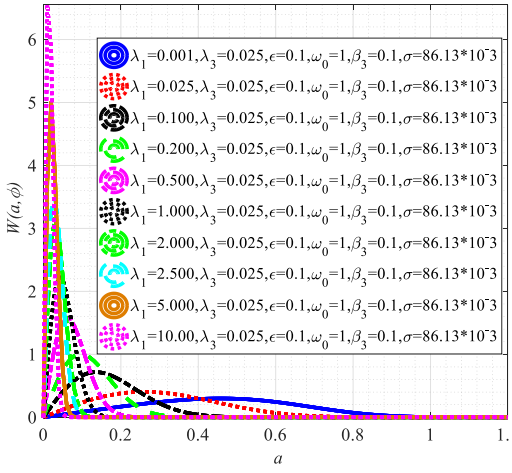

Fig. 4. $W(a,\phi)$ contours on the aW-plane with $\sigma = 86.13 \times 10^{-3}$ and λ_1 varies

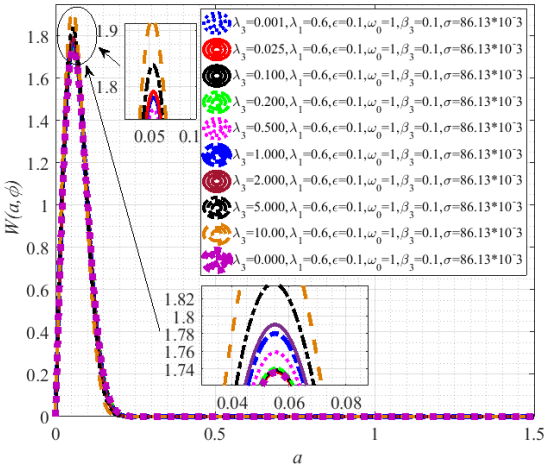

Fig. 5. $W(a,\phi)$ contours on the aW-plane with $\sigma = 86.13 \times 10^{-3}$ and λ_3 varies

As seen in Table 2, when the white noise intensity σ increases in the range of (53.80–3445.2)$\times 10^{-4}$, referring to the road roughness from a very good state to a very poor state, the approximate mean-square displacements corresponding to the first-, second-,

and third-order HOSA, say $\langle x^2 \rangle_1$, $\langle x^2 \rangle_2$, $\langle x^2 \rangle_3$, also increase in the range (0.121–488.62) $\times 10^{-4}$, respectively, which are closed to the Monte Carlo results. In detail, the maximum errors of $\langle x^2 \rangle_1$, $\langle x^2 \rangle_2$, $\langle x^2 \rangle_3$ are 0.9926%, 0.4673%, and 0.4015%, respectively. For road classes from A to D, the accuracies of $\langle x^2 \rangle_2$, $\langle x^2 \rangle_3$ are the same, and the accuracy of $\langle x^2 \rangle_3$ is better than that of $\langle x^2 \rangle_2$ as the road roughness becomes large. Meanwhile, the accuracy of $\langle x^2 \rangle_1$ is always less than that of $\langle x^2 \rangle_2$, $\langle x^2 \rangle_3$ as the road roughness varies from class B.

4. CONCLUSIONS

In the paper, the HOSA is applied to the analysis of an SDOF quarter-car model with cubic damping and stiffness subjected to a white noise base excitation. The works and conclusions can be summarized as follows:

The HOSA procedure for determining the second- and third-order PDFs is established. It is shown that the cubic stiffness term is lost in the first-order averaging procedure but preserved in the second- and third-order HOSA.

Numerical examination with the variations of linear and nonlinear damping coefficients regarding ISO road roughness classes is carried out. The Monte Carlo simulation is also performed to determine the mean-square values of the sprung mass displacement which is used as the exact solution for comparing with the approximate ones obtained from the first-, second-, and third-order stochastic averaging procedures. The results show that the accuracy of the third-order HOSA is the best, followed by the second-order one, and the first-order averaging procedure is the last.

The high accuracy of the HOSA shows its ability to investigate wider applications in other engineering problems.

DECLARATION OF COMPETING INTEREST

The authors declare that they have no known competing financial interests or personal relationships that could have appeared to influence the work reported in this paper.

FUNDING

This research received no specific grant from any funding agency in the public, commercial, or not-for-profit sectors.

REFERENCES

[1] A. Khazaie, N. Hussaini, H. Marzbani, and R. N. Jazar. Quarter car suspension model with provision for loss of contact with the road. In *Nonlinear Approaches in Engineering Applications*,

Springer International Publishing, (2018), pp. 167–208. https://doi.org/10.1007/978-3-319-69480-1_7.

[2] S. Yang, L. Chen, and S. Li. *Dynamics of vehicle-road coupled system*. Springer Berlin Heidelberg, (2015). https://doi.org/10.1007/978-3-662-45957-7.

[3] J. C. Dixon. *The shock absorber handbook*. Wiley, (2007). https://doi.org/10.1002/9780470516430.

[4] N. Panananda, N. S. Ferguson, and T. P. Waters. The effect of cubic damping in an automotive vehicle suspension model. In *International Symposium on the Computational Modelling and Analysis of Vehicle Body Noise and Vibration*, Brighton, United Kingdom, (2012).

[5] Z. Lozia and P. Zdanowicz. Optimization of damping in the passive automotive suspension system with using two quarter-car models. *IOP Conference Series: Materials Science and Engineering*, **148**, (2016), p. 012014. https://doi.org/10.1088/1757-899x/148/1/012014.

[6] M. Silveira, P. Wahi, and J. C. M. Fernandes. Effects of asymmetrical damping on a 2 dof quarter-car model under harmonic excitation. *Communications in Nonlinear Science and Numerical Simulation*, **43**, (2017), pp. 14–24. https://doi.org/10.1016/j.cnsns.2016.06.029.

[7] S. Li, S. Yang, and W. Guo. Investigation on chaotic motion in hysteretic non-linear suspension system with multi-frequency excitations. *Mechanics Research Communications*, **31**, (2004), pp. 229–236. https://doi.org/10.1016/j.mechrescom.2003.10.002.

[8] U. v. Wagner. On non-linear stochastic dynamics of quarter car models. *International Journal of Non-Linear Mechanics*, **39**, (2004), pp. 753–765. https://doi.org/10.1016/s0020-7462(03)00039-8.

[9] M. Silveira, J. M. Balthazar, and J. C. Moraes Fernandes. Stochastic analysis of 1-DOF vehicle suspension system employing asymmetrical damping. In *Proceedings of the 24th ABCM International Congress of Mechanical Engineering*, ABCM, COB17, (2017). https://doi.org/10.26678/abcm.cobem2017.cob17-0150.

[10] Y. A. Mitropolskii, N. V. Dao, and N. D. Anh. Nonlinear oscillations in systems of arbitrary order. *Naukova-Dumka, Kiev*, (1992). (in Russian).

[11] N. D. Anh. Higher order averaging method of coefficients in Fokker-Planck equation. *Sadhana*, **20**, (1995), pp. 373–387. https://doi.org/10.1007/bf02823197.

[12] N. D. Anh, N. N. Linh, N. N. Hieu, N. Van Manh, and A. T. Nguyen. Application of high order averaging method to Van der Pol oscillator. In *Advances in Asian Mechanism and Machine Science*, Springer International Publishing, (2021), pp. 825–834. https://doi.org/10.1007/978-3-030-91892-7_79.

[13] N. V. Manh, N. N. Linh, A. T. Nguyen, and N. D. Anh. Higher-order averaging procedure for performance analysis of a mono-stable Duffing piezoelectric energy harvesting system under white noise excitation. *Mechanics Research Communications*, **131**, (2023), p. 104157. https://doi.org/10.1016/j.mechrescom.2023.104157.

[14] C. J. Dodds and J. D. Robson. The description of road surface roughness. *Journal of Sound and Vibration*, **31**, (2), (1973), pp. 175–183. https://doi.org/10.1016/s0022-460x(73)80373-6.